Available online at www.sciencedirect.com
ScienceDirect
Deep-Sea Research I 54 (2007) 510–532
DEEP-SEA RESEARCH PART I
www.elsevier.com/locate/dsri

Formation and export of deep water in the Labrador and Irminger Seas in a GCM

Julie Deshayes[a,*], Claude Frankignoul[a], Helge Drange[b,c,d,e]

[a]LOCEAN, IPSL, Université Pierre et Marie Curie - Paris 6, Paris, France
[b]Nansen Environmental and Remote Sensing Centre, Bergen, Norway
[c]Bjerknes Centre for Climate Research, University of Bergen, Bergen, Norway
[d]Geophysical Institute, University of Bergen, Bergen, Norway
[e]Nansen-Zhu International Research Centre, Beijing, China

Received 21 March 2006; received in revised form 14 December 2006; accepted 29 December 2006
Available online 31 January 2007

Abstract

The influence of changes in the rate of deep water formation in the North Atlantic subpolar gyre on the variability of the transport in the Deep Western Boundary Current is investigated in a realistic hind cast simulation of the North Atlantic during the 1953–2003 period. In the simulation, deep water formation takes place in the Irminger Sea, in the interior of the Labrador Sea and in the Labrador Current. In the Irminger Sea, deep water is formed close to the boundary currents. It is rapidly exported out of the Irminger Sea via an intensified East Greenland Current, and out of the Labrador Sea via increased southeastward transports. The newly formed deep water, which is advected to Flemish Cap in approximately one year, is preceded by fast propagating topographic waves. Deep water formed in the Labrador Sea interior tends to accumulate and recirculate within the basin, with a residence time of a few years in the Labrador Sea. Hence, it is only slowly exported northeastward to the Irminger Sea and southeastward to the subtropical North Atlantic, reaching Flemish Cap in 1–5 years. As a result, the transport in the Deep Western Boundary Current is mostly correlated with convection in the Irminger Sea. Finally, the deep water produced in the Labrador Current is lighter and is rapidly exported out of the Labrador Basin, reaching Flemish Cap in a few months. As the production of deep-water along the western periphery of the Labrador Sea is maximum when convection in the interior is minimum, there is some compensation between the deep water formed along the boundary and in the interior of the basin, which reduces the variability of its net transport. These mechanisms which have been suggested from hydrographic and tracer observations, help one to understand the variability of the transport in the Deep Western Boundary Current at the exit of the subpolar gyre.

Keywords: North Atlantic subpolar gyre circulation; Labrador Sea Water; Convection; Deep water spreading; Deep Western Boundary Current; Interannual variability

1. Introduction

The oceanic Meridional Overturning Circulation (MOC) and the associated poleward heat transport contribute substantially to the present energy balance of the Earth (Trenberth and Caron, 2001).

*Corresponding author. WHOI, MS #21, Woods Hole, MA 02543, USA.
E-mail address: jdeshayes@whoi.edu (J. Deshayes).

0967-0637/$ - see front matter © 2007 Elsevier Ltd. All rights reserved.
doi:10.1016/j.dsr.2006.12.014

One fundamental driver of the MOC is the formation of intermediate to deep water masses in the northern North Atlantic resulting from the winter densification of the surface water. The variability of the MOC can be related to changes in the rate of deep water formation in the northern North Atlantic in simulations with oceanic General Circulation Models (GCMs) (Eden and Willebrand, 2001; Bentsen et al., 2004; Mignot and Frankignoul, 2005). Coupled climate GCMs suggest that the MOC is highly sensitive to surface salinity perturbations in the regions of formation of intermediate to deep water (e.g., Manabe and Stouffer, 1995; Stouffer et al., 2006): an anomalous input of freshwater will reduce the deep water formation rate, resulting in a weakening of the Atlantic MOC. This will tend to reduce the poleward heat transport and have therefore considerable impact on, in particular, the Atlantic-European climate (e.g., Vellinga and Wood, 2002). However, the link between changes in the rate of deep water formation and the variability of the MOC is not clearly established. For instance, Mauritzen and Häkkinen (1999) suggested that changes in the rate of deep water formation might not affect the MOC but influence the characteristics of the water masses at depth. The role of the wind-driven circulation is also unclear, and Straneo (2006) suggested that the overturning and the poleward heat transport might vary because of changes in the wind-forced circulation even if the rate of deep water formation remains unchanged.

The deep water formed in the North Atlantic is mostly carried southward by the Deep Western Boundary Current (DWBC), which constitutes the lower limb of the Atlantic MOC. The DWBC originates from the southward slopes of the Greenland–Scotland Ridge, and in the Irminger and Labrador Seas (Dickson and Brown, 1994, see the location of these geographical features in Fig. 1). Once formed, the DWBC follows the topography along the western boundary of the North Atlantic basin. The densest water masses are formed in the Nordic (Greenland, Iceland and Norwegian) Seas and in the Arctic Ocean, and overflow through the deepest sills of the Greenland–Scotland Ridge. The lighter water masses are formed in the Labrador Sea (therefore called Labrador Sea Water, LSW) and in the Irminger Sea (Pickart et al., 2003; Bacon et al., 2003). Although the characteristics of the DWBC and its variations on the monthly timescale have been described (e.g., Lazier and Wright, 1993; Fischer et al., 2004), its interannual variability remains poorly documented because of the scarce-

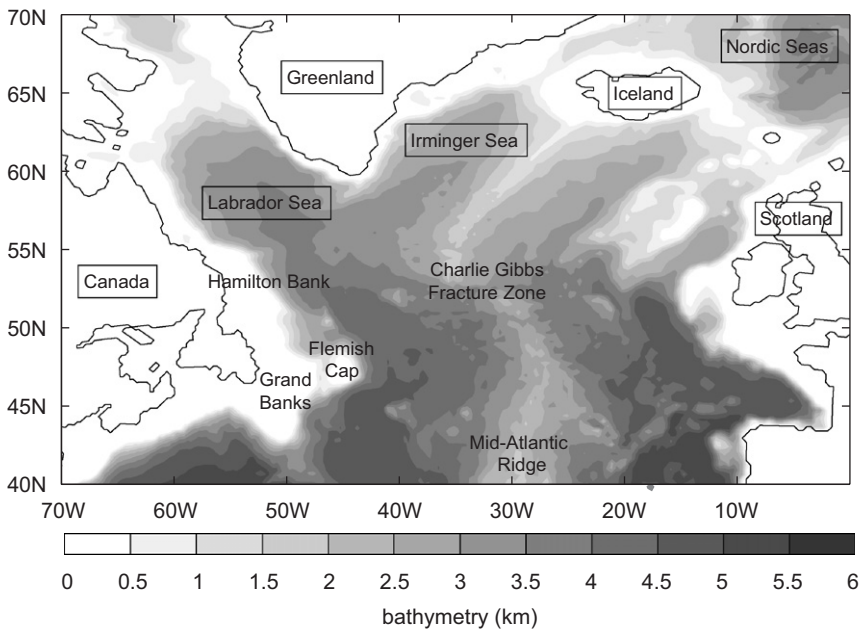

Fig. 1. Bathymetry of the model between 40°N and 70°N (based on the ETOPO-5 data base, Data Announcement 88-MGG-02, Digital relief of the Surface of the Earth, NOAA, National Geophysical Data Center, Boulder, Colorado, 1988) and location of key geographical features in the North Atlantic.

ness of tailored and long-term observations, and so does its link with changes in the rate of deep water formation. The repeated observations of Schott et al. (2004) reveal that the DWBC transport in the region of the Grand Banks hardly varied in two surveys 6 years apart, although the convection activity had changed a lot during that period. Downstream of the Grand Banks, the transport in the DWBC seems to be mostly influenced by the Gulf Stream (Bower and Hunt, 2000), topographic Rossby waves and recirculation cells (Pickart and Watts, 1990).

In order to understand the connection between deep water formation and the transport in the DWBC, it is essential to clarify the timescale and pathways of the export of the newly formed deep water out of the subpolar gyre. Straneo et al. (2003) have shown, using an advective–diffusive model based on lagrangian drifter data in the Labrador Sea, that the mean interior flow field in the Labrador Sea plays an important role in the export of LSW. The interior circulation in the Labrador Sea consists of large recirculation cells adjacent to the cyclonic boundary currents (Lavender et al., 2000; Fischer et al., 2004), which are mainly forced by the wind (Käse et al., 2001; Spall and Pickart, 2003). The residence time of LSW in the Labrador Sea is estimated to be 4–5 years, which suggests that the Labrador Sea acts as a reservoir for newly formed LSW, while LSW formed in the Irminger Sea seems to be directly exported out of the subpolar gyre by the intense boundary currents (Cuny et al., 2002). The timescale of the LSW export thus depends on whether convection occurred in the Labrador or Irminger Seas.

Deep water formation has also been observed in the boundary current of the Labrador Sea (Pickart et al., 1997; Cuny et al., 2005). The newly formed water masses are lighter than those produced in the interior and are called upper LSW (uLSW), by opposition to the classical LSW (cLSW) formed in the Labrador Sea interior and in the Irminger Sea. Studies based on CFC-11 inventories showed that uLSW is an important constituent of the DWBC (Smethie and Fine, 2001), and that it can also be produced in the central Labrador Sea when the formation of cLSW is reduced (Stramma et al., 2004). Indeed, Kieke et al. (2006) found that the lack of cLSW formation in the late 1990s was compensated by the formation of uLSW.

In this paper we use a hind cast simulation of the circulation in the North Atlantic from a state-of-the-art oceanic GCM to explore the link between the formation and export of deep water in the Labrador and Irminger Seas and the variability of the DWBC transport.

2. Description of the simulation

2.1. The model

The oceanic GCM used in this study is the Nansen Center (Bentsen et al., 2004; Drange et al., 2005) version of the Miami Isopycnic Coordinate Ocean Model MICOM (Bleck et al., 1992). The regional model covers the North Atlantic from 30°N to 78°N, and it has a horizontal resolution of about 20 km in the region of interest. In the vertical, the model has 26 density layers. The upper model layer represents a vertically uniform mixed layer (ML), with variable temperature and salinity, and hence density. The 25 layers below the ML have constant potential density (given in Table 1) but variable thickness and temperature. The simulated layer salinity is then diagnosed based on the simplified equation of state by Friedrich and Levitus (1972). Sea ice dynamics and thermodynamics are represented by the model of Harder (1996) and Drange and Simonsen (1996), respectively. Isopycnal diffusive velocities for layer interface, momentum and tracer dispersion are, respectively, $0.02\,m\,s^{-1}$, $0.025\,m\,s^{-1}$ and $0.015\,m\,s^{-1}$, yielding isopycnal diffusivities of the order of $10^3\,m^2\,s^{-1}$. Diapycnal mixing is parameterized as a function of stratification by $K_d = 3 \times 10^{-7} N^{-1}$ ($m^2\,s^{-1}$), where N is the Brunt–Väisälä frequency.

At the lateral boundaries, the regional model is relaxed toward a global 40 km version of the same model by means of one way nesting. The global model fields are read once a week and interpolated in time to specify the relaxation boundary condi-

Table 1
Potential density of the layers below the mixed layer in the model, in σ_0 unit ($kg\,m^{-3}$)

Layer	2	24.12	11	27.38	20	27.98
	3	24.70	12	27.52	21	28.01
	4	25.28	13	27.63	22	28.04
	5	25.77	14	27.71	23	28.07
	6	26.18	15	27.77	24	28.10
	7	26.52	16	27.82	25	28.85
	8	26.80	17	27.86	26	29.10
	9	27.03	18	27.90		
	10	27.22	19	27.94		

tions for the regional model at each time step. The global model was spun up for 85 years by applying monthly climatological (for 30 years) then daily (from 1948 to 2003) NCEP/NCAR reanalysis fields, using the scheme of Bentsen and Drange (2000). The global simulation at the end of the spin up was interpolated and used as the initial condition for the regional simulation. The regional and the global simulations were then both forced with the daily mean NCEP/NCAR reanalysis fields from 1948 to 2003. Although there was no other restoring than that inherent to the turbulent heat flux formulation in the global model, the ML temperature and salinity fields of the regional model were linearly relaxed towards the monthly mean climatological values of Levitus and Boyer (1994) and Levitus et al. (1994), respectively, as described in Bentsen et al. (2004). The relaxation scheme has been shown to be sufficiently weak to allow for seasonal to interannual variations in the simulated hydrography in the northern North Atlantic (Hátún et al., 2005a, b).

2.2. Influence of the boundary conditions

The mean circulation and the hydrography in the global model are reasonably realistic, except that convection in the Labrador Sea is too shallow and convection in the Irminger Sea is overestimated. This seems to result from too low a salinity in the interior of the Labrador Sea and too low a temperature in the interior of the Irminger Sea in winter. These biases are transmitted to the regional model, but they are largely compensated by a too cold temperature in the interior of the Labrador Sea, which yields deeper convection in that region, and too low salinity in the interior of the Irminger Sea, which reduces convection there. Hence, horizontal resolution does not seem to influence directly the depth of convection, consistent with Treguier et al. (2005). On the other hand, the circulation of the nested model is improved by the higher resolution, except in the subtropical gyre (see below).

Near the boundaries of the regional model, the variability of temperature and salinity is largely constrained by the global simulation. The latter may not have reached equilibrium in the Nordic Seas, as there is a slow increase of salinity below 2000 m depth. Near the southern limit of the regional model, salinity and temperature tend to decrease in the upper 500 m and increase below, while further east a freshening develops at depth after 1973. Again, this may be in part due to model drift. However, it does not seem to strongly affect the subpolar gyre, where salinity tends to decrease at depth and increase near the surface, which corresponds to the observations (Curry and Mauritzen, 2005), as will be discussed elsewhere. It is therefore not expected that the low frequency variability of the subpolar gyre, which is the focus of this study, is degraded by model drift.

2.3. Mean circulation

In this paper, we focus on the circulation in the subpolar North Atlantic (approximately from 47°N to 67°N) from January 1953 to December 2003. The surface circulation (Fig. 2a) compares well with the observations (Reverdin et al., 2003). However, the subtropical gyre is too weak and the Gulf Stream too broad, following the 1000 m isobath as far north as Flemish Cap before leaving the coast. Hence, the circulation is not realistic near the Grand Banks, reflecting the relatively low resolution of the model. Another discrepancy is that the North Atlantic Current flows eastward at approximately 48°N, which is more to the south than in observations.

In the simulation, a direct connection exists between the West Greenland Current and the Labrador Current near 59°N, which does not clearly appear in observations, although it has been suggested by the propagation of surface drifters (Cuny et al., 2002). The Labrador Current is formed of two branches near the Hamilton Bank. One closely follows the coast as a continuation of the Baffin Island Current. The other follows the 1000 m isobath until a recirculation cell forms, creating a northward current at 55°N, 48°W that either turns west toward the interior of the Labrador Sea, or east toward the interior of the Irminger Sea (Fig. 2a). This can be seen as a wide recirculation cell which goes from the interior of the Labrador Sea to the interior of the Irminger Sea. Spall and Pickart (2003) have shown that this recirculation cell is mainly influenced by wind-forcing and topography.

The transport of dense water across the Greenland–Scotland Ridge is much weaker than in observations: the total transport is 1.8 Sv for $\sigma_0 \geqslant 27.86\,\mathrm{kg\,m^{-3}}$, to be compared to 5.6 Sv for $\sigma_\theta \geqslant 27.80\,\mathrm{kg\,m^{-3}}$ (Dickson and Brown, 1994). As a result, the circulation of dense water coming from the Nordic Seas is not realistic and will not be studied further.

The recirculation from the Labrador Current to the West Greenland Current and the Irminger Sea is

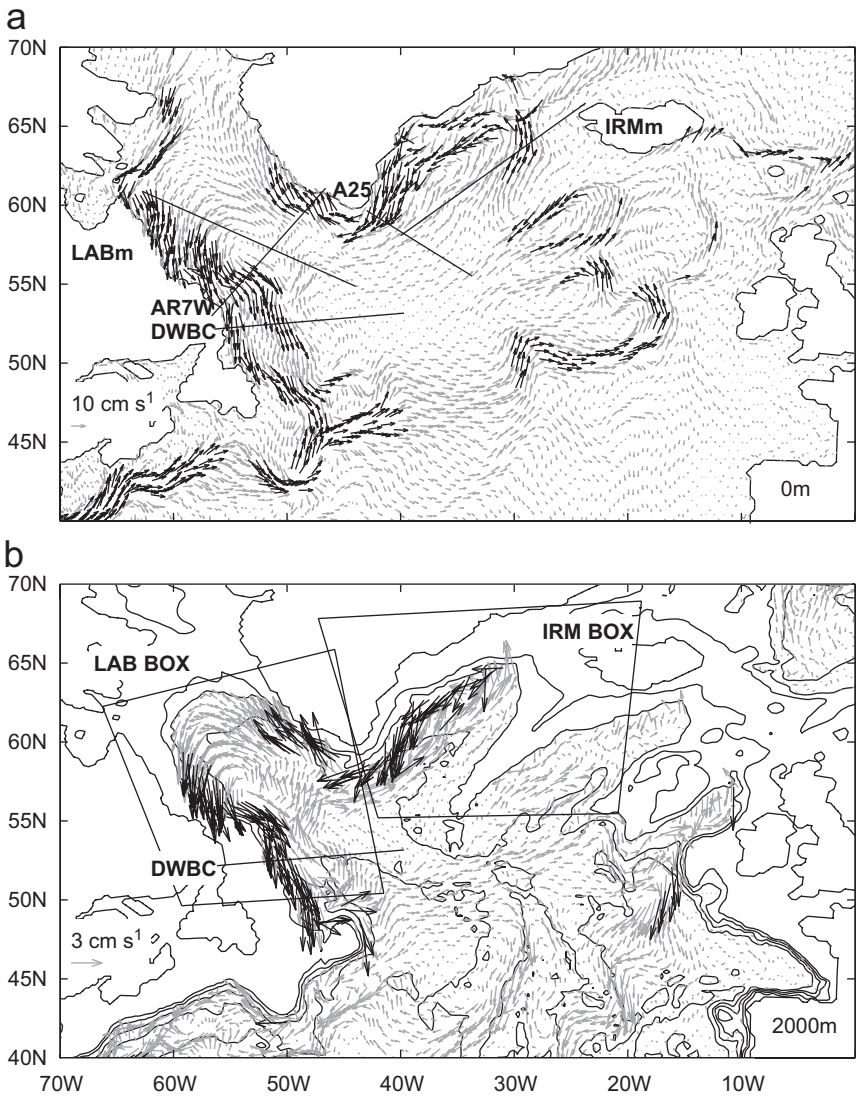

Fig. 2. Mean circulation at the surface (a) and 2000 m depth (b). Arrows representing currents of amplitude larger than 10 cm s^{-1} are colored in black and rescaled to a fixed length. Only 1 of 4 vectors is represented. The black lines indicate the location of sections A25, IRMm, AR7W, LABm and DWBC (a), and the 1000, 2000, 3000, 4000 and 5000 m isobaths (b). Boxes IRM and LAB are used to estimate the rate of deep water formation in the Irminger and Labrador Seas.

also present at 2000 m depth (Fig. 2b), which seems realistic as Talley and McCartney (1982) determined that LSW is advected northeastward into the Irminger Sea. In the circulation scheme obtained by Lavender et al. (2000) at 700 m depth, a counter-current flows parallel and opposite to the Labrador Current, the West Greenland Current and the East Greenland Current. Based on Lavender et al. (2000), the northward part of the counter-current in the Labrador Sea is located near 59°N, 55°W, while in the simulation it is found near 55°N, 48°W. Fischer and Schott (2002), using *in situ* measurements, also describe a weak anticyclonic recirculation adjacent to the southeastward Labrador Current (their Fig. 4b).

In the simulation, the DWBC originates in the Irminger Sea, hence does not carry dense water coming from the eastern part of the North Atlantic through the Charlie Gibbs Fracture Zone as in the observations (Dickson and Brown, 1994). It flows along the eastern topography of Greenland and along the topography around the Labrador Sea as far as Flemish Cap (Fig. 2). The observations show that the deep water masses in the North Atlantic

Current differ from those in the DWBC (Schott et al., 2004). Because the Gulf Stream remains too close to the coast in the simulation, the North Atlantic Current only detaches from the coast at the Flemish Cap. Hence, most of the DWBC flows northeastward at Flemish Cap, toward the Mid-Atlantic Ridge. On its western flank, part of this current turns southward and forms an intense jet along the topography that eventually turns southwestward. Part of the northeastward current goes through the Charlie Gibbs Fracture Zone and forms an intense jet on the eastern flank of the Mid-Atlantic Ridge. P-ALACE floats have been reported to pass through the Mid-Atlantic Ridge at 700 m (Lavender et al., 2000) and 1500 m (Fischer and Schott, 2002; Schott et al., 2004) depth, and the presence of LSW in the eastern North Atlantic has been observed repeatedly (e.g., Cunningham and Haine, 1995). The observed circulation (e.g., Paillet et al., 1998) appears less intense than in the simulation, but the southward pathways for subpolar deep water at 30°W and 20°W have been suggested from observations (Schott et al., 2004).

The spatial distribution of eddy kinetic energy at the surface corresponds well to the observed one (Reverdin et al., 2003), but its amplitude is about one order of magnitude too small (not shown), likely because of the limited horizontal resolution of 20 km and the lack of vertical shear in the ML, which prevents baroclinic instabilities (e.g., Eldevik, 2002). The weak eddy kinetic energy results in too weak turbulent mixing and reduces the influence of the warm and salty subtropical water advected by the boundary currents, on the interior of the Labrador and Irminger Seas. This may explain why the surface isotherms and isohalines are parallel to the boundary currents, and why the interior of the Labrador and Irminger Seas are 1–2 °C too cold and 0.3 too fresh (Fig. 3). The eddy kinetic energy at depth is also one order of magnitude smaller than in observations (not shown). The ice cover in the simulation is restricted to the northern Irminger Sea and to an area along the Labrador coast (Fig. 3b), in general accordance with available observations.

At depth, the winter hydrography shown along WOCE section AR7W (Fig. 4 a,c, see location in Fig. 2) is in general agreement with snapshot observations (e.g., Pickart and Torres, 2002) and Hydrobase-2 climatology (from Curry, 2006, http://www.whoi.edu/science/PO/hydrobase) except that the temperature is approximately 1.5 °C too cold

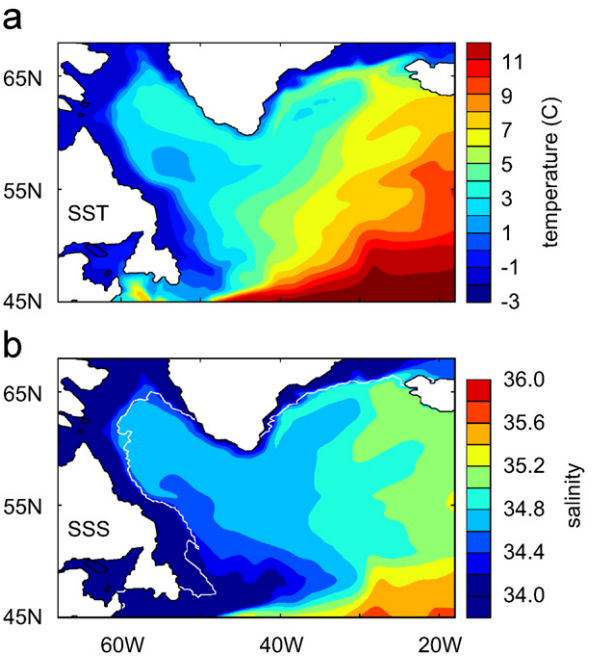

Fig. 3. Mean surface temperature (a) and salinity (b) in winter (February–April). The maximum extent of ice cover is indicated by the white line in panel (b).

and the salinity 0.2 too low in the simulation. However, the patterns are similar. Note that the warm and salty water masses carried by the West Greenland Current are hardly visible in the Labrador Current due to mixing with fresh and cold water masses coming from the Baffin and Hudson Bays, consistent with observations (e.g., Cuny et al., 2002). Along WOCE section A25 (Fig. 4, b,d), the temperature is again 1.5 °C too cold and the salinity 0.2 below the observed values (Krauss, 1995, Hydrobase-2), but the patterns are similar to observations, except at depth presumably because of failures in the representation of the overflow water masses coming from the Nordic Seas.

Although there are biases in the mean temperature and salinity distributions, this may not influence the variability. At the beginning of the simulation, the salinity anomalies along sections AR7W and A25 differ from the observed ones, presumably because the model simulation starts in 1948 (with the availability of atmospheric reanalysis fields). The comparison improves with time and by the late 1960s the salinity anomalies become more realistic. Salinity and temperature slowly decrease at depth since 1973, the anomalies being largest from 1500 to 3000 m, while they increase near the surface and in the boundary currents, mostly since 1990.

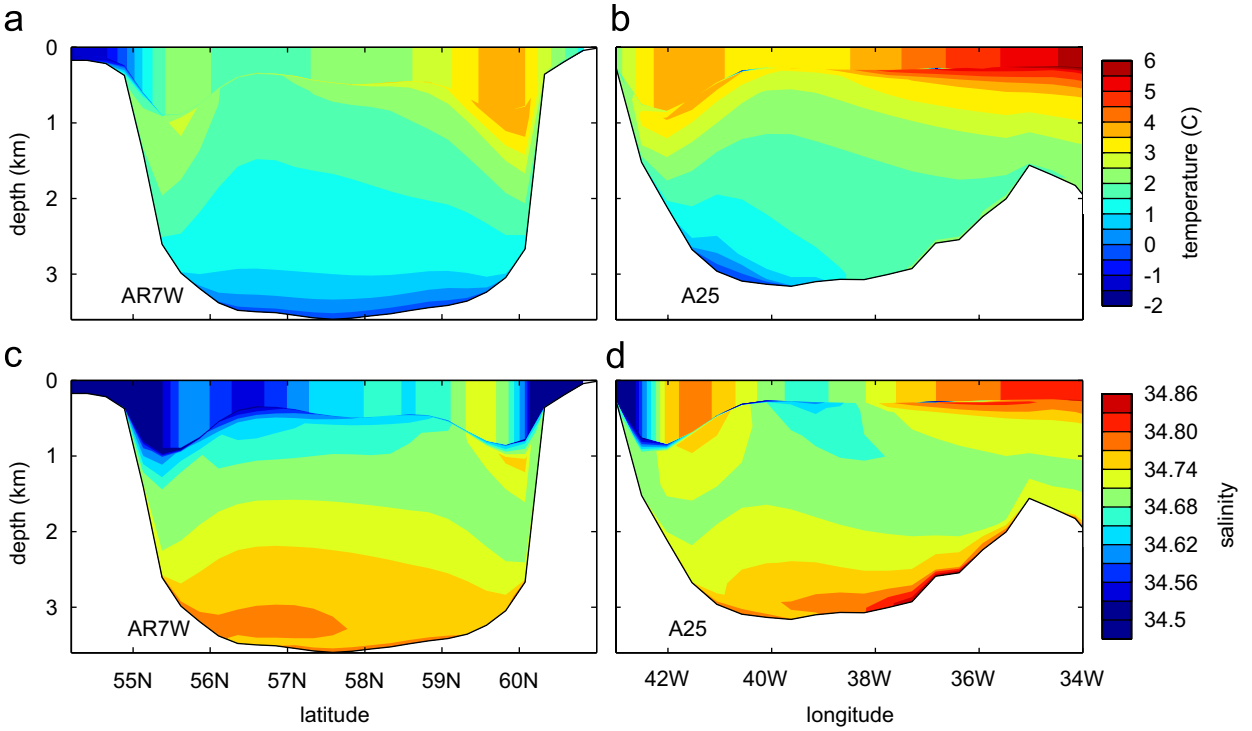

Fig. 4. Mean temperature (a,b) and salinity (c,d) along sections AR7W (a,c) and A25 (b,d) in winter.

Finally, density slightly increases since 1973 from the surface to 2500 m depth in the interior of the Labrador and Irminger Seas but slightly decreases in the boundary currents and above the Reykjanes Ridge and below 2500 m depth presumably because of a drift in the simulation.

3. Deep water formation

3.1. Mixed layer variability

In winter, the mean ML is deepest in regions close to the coast where the surface boundary currents are intense: in the Irminger Current, the East Greenland Current, and the Labrador Current (Fig. 5a). In these regions, the winter ML thickness exhibits a strong interannual variability (Fig. 5b). However, the standard deviation is maximum away from the coast, in the northern interior of the Irminger Sea and in the southwestern interior of the Labrador Sea. Because the regions where the mean winter ML is deepest are not those where the winter ML thickness varies most, as in the observations, we adopt two criteria to identify the regions of deep water formation, instead of one as in Bentsen et al. (2004).

The first criterion selects regions where the ML is sufficiently deep on the average to produce dense water. In the Labrador Sea, an area where the mean winter ML is thicker than 1100 m is identified and labeled LABb (Fig. 5a). The mean winter ML is also thick in the East Greenland Current but it is much shallower than in the Labrador Current, suggesting that the subsequent formation of intermediate and deep water is less important. The fact that the ML deepens most where the surface current is intense is consistent with other simulations based on isopycnal models (Willebrand et al., 2001). Observations show that convection takes place within the Labrador Current, but only sporadically (Pickart et al., 1997; Cuny et al., 2005). This indicates that boundary convection is overestimated in the simulation.

The second criterion identifies regions where the ML thickness changes a lot at the interannual timescale. Area LABi (respectively, IRMi) is defined as where the standard deviation of the winter ML thickness exceeds 480 m (310 m) in the Labrador (Irminger) Sea (Fig. 5b), but note that the results below do not depend on the precise definition of the areas. The region LABi is located within the Labrador Sea gyre and corresponds to the observed

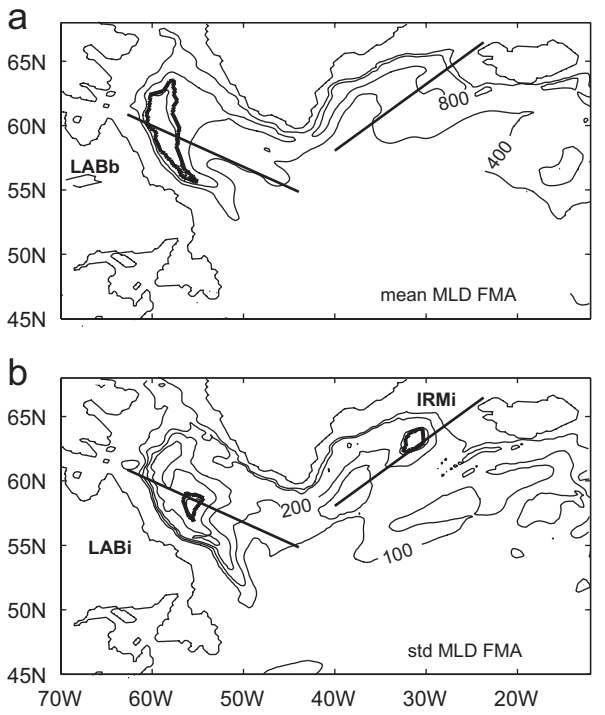

Fig. 5. Mean thickness (a, from 400 m in 400 m intervals) and standard deviation (b, from 100 m in 100 m intervals) of the mixed layer in winter (February–April) and location of areas LABb, IRMi and LABi. The thin straight lines indicate the location of sections LABm and IRMm.

region of convection in the Labrador Sea (Marshall and Schott, 1999). The newly formed water masses are thus likely to remain largely trapped within the gyre, which is consistent with observations (Straneo et al., 2003). On the other hand, area IRMi is located in the northeastern part of the Irminger Sea while the observations imply that convection occurs in the southwestern part of the basin (Pickart et al., 2003; Bacon et al., 2003). This is likely caused by the limited resolution of the ocean model and of the atmospheric forcing that does not represent small-scale phenomena such as the East Greenland tip jet (Pickart et al., 2003). Besides, in the simulation, the southern interior of the Irminger Sea is too fresh, because of the lack of horizontal mixing with the saltier subtropical water masses, which inhibits convection there. The Irminger Sea convection thus takes place in the northern part of the basin, too close to the boundary current, resulting in a fast export of the newly formed water masses, as discussed below. Although likely model dependent, the mechanism of variability associated with convection and export of the newly formed deep water in the Irminger Sea is interesting as it contrasts with that in the Labrador Sea (see below).

The time series of the thickness of the ML in the regions of convection are given in Fig. 6 (a,c,e). For

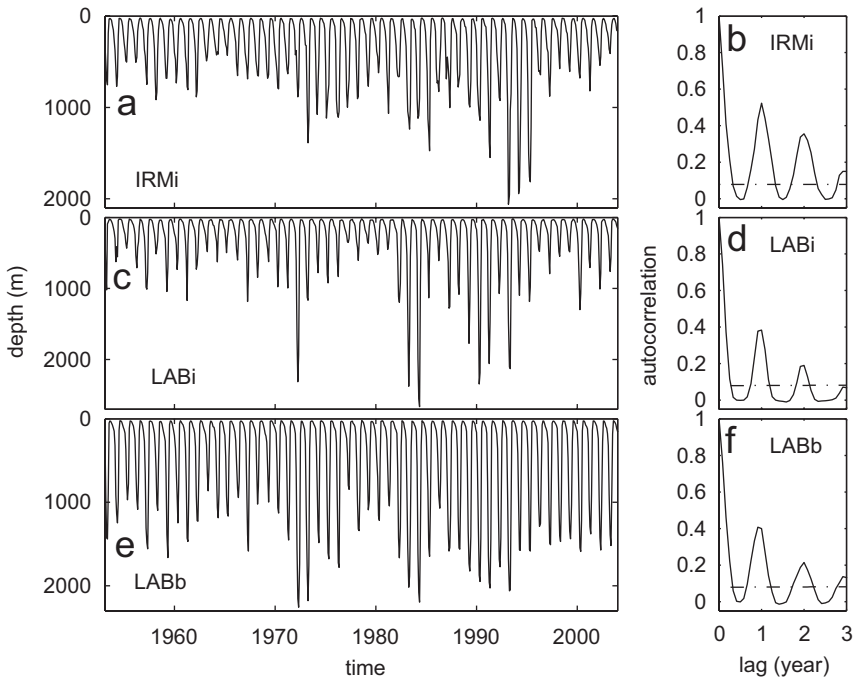

Fig. 6. Thickness of the mixed layer in the regions of convection (a,c,e) and autocorrelation of the monthly anomalies (b,d,f). The dash-dotted lines indicate the 5% significance level for uncorrelated normal samples.

the three regions, the ML is deepest in winter (February–April). In LABi, the winter ML is relatively shallow in the early part of the simulation but deep in 1972, 1983, 1984, from 1989 to 1991, and in 1993, which corresponds well to observations (Lazier, 1980, 1995; Lazier et al., 2002), suggesting that the temporal variability of the model is realistic. The ML depth in LABb is highly correlated with that in LABi ($r = 0.82$), although the former has much less interannual variability. In the Irminger Sea, the ML is also relatively shallow at the beginning of the simulation. Convection occurs in 1973, 1985, 1991, and from 1993 to 1995, so that the ML depth in IRMi is correlated with that in LABi when LABi leads IRMi by 1 year ($r = 0.61$). Note that in the three regions of convection the ML depth anomalies show some persistence from one winter to the next, which results in a peak of their autocorrelation at a lag of 1, 2, and even 3 years (Fig. 6, b,d,f).

3.2. Displacements of the isopycnals at depth

To characterize the circulation and the density when deep water formation occurs in the Irminger Sea, a composite of convection events is constructed from the years when the winter ML in IRMi exceeds 1150 m (1973, 1985, 1991, 1993–1995). Fig. 7 shows the corresponding current normal to and the isopycnals along section IRMm (see location in Fig. 2). The normal current is maximum along the continental slope, where it is oriented westward, and minimum in the interior of the basin. Only small seasonal changes are seen for these features. In winter (a), the ML thickness is close to 1000 m in the boundary current, increasing to 1500 m at 31.5°W, just offshore from the boundary current, and then decreasing further southward. The ML is densest where it is deepest, its density reaching that of layer 14, whose thickness essentially vanishes below the ML. The thickness of layer 15 is also much thinner around 31.5°W than further south. During the summer following the convective events (b), the isopycnals at depth are almost flat away from the boundary current, and their positions correspond to those in winter at the southern edge of the section. Hence the water masses formed in winter, seaward of the intense boundary current, seem to spread laterally in summer with little change in volume.

A composite was similarly constructed for the convection events in the Labrador Sea when the

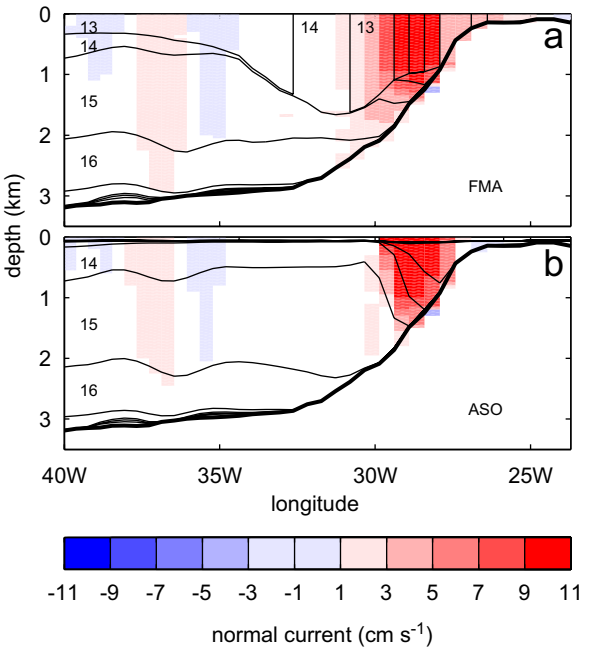

Fig. 7. Composite of the current normal (positive northwestward) to section IRMm (color) and isopycnals (black lines) in February–April (FMA, a) and August–October (ASO, b) during deep-convection in the Irminger Sea. Normal current is positive westward, and was interpolated on fixed vertical levels (resolution 50 m) before averaging. The isopycnal layers are identified by their number (see Table 1 for their potential density), except for the mixed layer, for which density was binned into the potential density of the layers at depth.

winter ML in LABi exceeds 1300 m (1972, 1983, 1984, 1989, 1990, 1991, 1993), which we refer to as a deep convection composite. To characterize the conditions when convection is shallower, we also average years 1953 to 1970 to form a shallow convection composite. The circulation and the position of the isopycnals at depth during deep and shallow convections are shown in Fig. 8 along section LABm (see Fig. 2). The circulation normal to section LABm is oriented southward from the coast to 53°W and northward from 52°W to 45°W, and is mostly intense in the boundary current. The circulation intensifies during deep convection, especially in the center of the Labrador Sea, near 55°W. During shallow convection (a,c panels), the ML is deepest just offshore from where the surface current is most intense, which corresponds to area LABb. Its density corresponds to that of layer 13, and is rather homogeneous along the section. There is little seasonal change in the thickness of the layers at depth, except for layer 14 which is a little thicker in

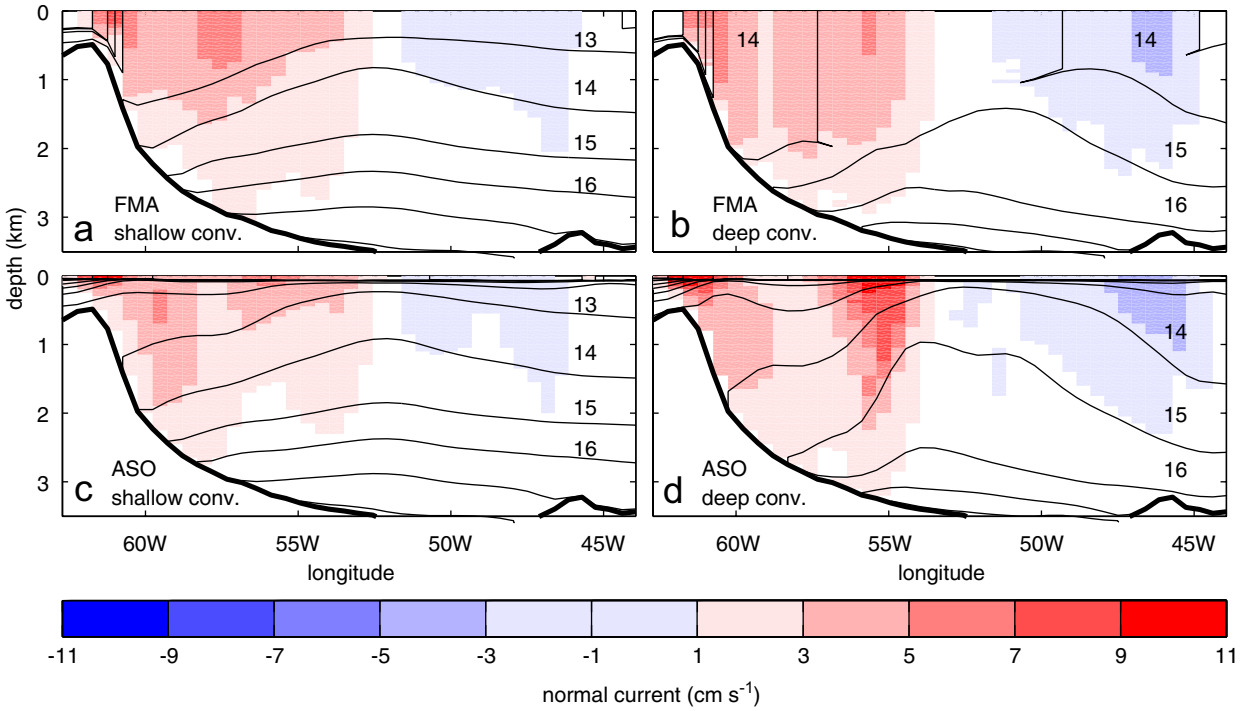

Fig. 8. Same as Fig. 7 for section LABm during shallow (a,c) and deep (b,d) convections in the Labrador Sea. Normal current is positive southward.

summer, which may indicate the formation of deep water of the corresponding density, even though the average density of the ML is only that of layer 13 (indeed the maximum ML density in winter in area LABb equals that of layer 16 on a weekly basis). During deep convection (b,d panels), the winter ML is densest from 57°W to 48°W, which includes area LABi, and by the following summer, layers 15 and 16 have become much thicker in the center of the Labrador Sea. The subsequent doming of the isopycnals is coherent with the intensification of the cyclonic circulation, but it is not clear whether they are due to convection or wind forcing. Note that during these events, the ML is also very deep in area LABb but somewhat lighter than in the interior, which explains why the time series of convection in LABi and LABb are highly correlated.

3.3. Correlation with the atmospheric forcing

In this paper, the emphasis is not on the causes of deep water formation but on the evolution of the newly formed water masses. Nonetheless, it is useful to briefly describe the link between convective mixing and the atmospheric forcing. The correlations are calculated between the anomalies of the ML volume in February, March and April in the areas of convection and the monthly anomalies of the other variables binned into corresponding or lagged groups of 3 months. The degrees of freedom are estimated from the autocorrelations of the monthly anomalies as in Bretherton et al. (1999). As shown in Fig. 9 (a,b, solid line), convection in LABi is well correlated with the local atmospheric heat flux ($r = 0.5$) when the latter leads convection by few months, while the correlation between convection in IRMi and the local heat flux is much smaller ($r = 0.25$), albeit significant.

Changes in the wind stress may alter the sea surface height, the surface currents, the doming of the isopycnals, and the deepening of the ML. A principal component analysis of the sea surface height monthly anomalies showed that the main modes of variability in the Irminger and Labrador Seas reflect changes in the cyclonic circulation. The first mode of variability in the Irminger Sea (which explains 56% of the variance) mainly describes, in this polarity, a low-frequency drop of the sea surface (hence a doming of the isopycnals) that is particularly strong in the northern boundary current (Fig. 9c). The associated principal component is well correlated with convection in IRMi in both lead and lag conditions (dashed

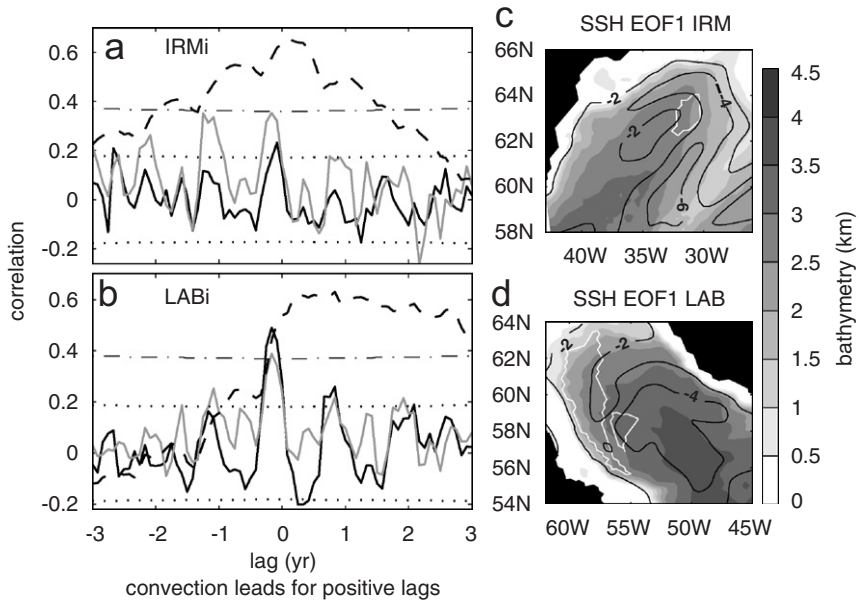

Fig. 9. Left: correlation of the monthly anomalies of the winter mixed layer volume in areas IRMi (a) and LABi (b) with the corresponding atmospheric heat fluxes (black solid lines), the principal components (PCs) of the first modes of variability of the sea surface height anomalies (dashed lines) and the NAO index (gray lines). The estimated 5% significance level is given by the dotted lines, except for the correlations with the PCs of the sea level changes, given by the dash-dotted lines. Right: spatial patterns of the first modes of variability (principal component analysis) of the sea surface height anomalies in the Irminger Sea (c) and in the Labrador Sea (d). The white lines indicate the location of areas IRMi, LABi and LABb, while the shading represents the bathymetry.

line in Fig. 9a), which is consistent with the 3 year decay time of convection. The time series of the sea level monthly anomalies is also well autocorrelated at a few years lag, presumably because the gyre circulation has most variance on the decadal time-scale (not shown). The good correlation when convection lags the sea level by up to a year or two suggests that the low-frequency doming of the isopycnals and the related intensification of the surface currents strongly precondition convection in IRMi, which is coherent with the position of area IRMi just offshore of the intense boundary current (Fig. 7). The correlation is also important for positive lags, and maximum when convection in IRMi leads sea level changes by a few months, suggesting that the deepening of the ML influences the surface currents and the sea surface height in return.

In the Labrador Sea, the first mode of sea level variability (which explains 42% of the variance) primarily describes low-frequency sea level changes in the center of the basin, with maximum amplitude close to area LABi (Fig. 9d). The associated principal component is well correlated with convection in LABi when sea level lags by a few months to several years, but it is uncorrelated when sea level leads by more than a few months (dashed line in Fig. 9b). This indicates that convection in LABi is not influenced by low-frequency preconditioning but instead directly driven by the atmospheric buoyancy forcing, as suggested above.

The atmospheric forcing in the Labrador and Irminger Seas is related to the North Atlantic Oscillation (Hurrell, 1995, hereafter NAO, the associated index is here defined as the normalized principal component of the first EOF of the sea level pressure monthly anomalies in the North Atlantic). A positive phase of the NAO increases the heat loss over the Labrador Sea and, via Ekman pumping (Marshall et al., 2001), decreases the cyclonic gyre circulation in the Labrador Sea and increases that in the northern Irminger Sea. As a result, convection in LABi and IRMi are both correlated with the NAO when the NAO leads by a few months (Fig. 9, a,b, gray lines). However, convection in IRMi is also correlated with the NAO when the latter leads by 1 year, presumably because of the preconditioning effect of the NAO-driven doming of the isopycnals discussed above. Note that the positive correlation of convection in LABi with the NAO indicates that direct wind forcing does not control

convection in LABi since the decrease of the cyclonic circulation near the convection site should decrease the isopycnal doming.

During the years of deep convection in the Irminger and Labrador Seas (which only slightly differ), the boundary currents are faster, indicating that the DWBC intensifies (Fig. 10). This results in a faster export of the newly formed deep water out of the subpolar gyre, which is discussed below. The northeastward current which goes from the Labrador Sea to the Irminger Sea is also more intense, especially at depth, indicating that the overall subpolar gyre circulation intensifies as well. To what extent these changes are due to deep water formation or to the direct response of the subpolar gyre circulation to wind forcing will be addressed in another paper.

3.4. Identification of convection products

The T–S diagram in Fig. 11 documents the characteristics of the various newly formed water masses by considering monthly averages in the mixed layer in winter. In area LABi, the ML temperature and salinity range from 0.7−3.2 °C and from 34.55 to 34.7, respectively (Fig. 11a). The ML is coldest and saltiest when it is deep, hence when convection occurs, and the average temperature and salinity for the composite event of convection in LABi equal 1.3 °C and 34.68, respectively. If one takes into account the −2 °C and −0.2 biases in temperature and salinity in the interior of the Labrador Sea, this is consistent with the characteristic temperature and salinity of cLSW in observations, ranging from 2.8 to 3.6 °C and from 34.83 to 34.90, respectively (Lazier, 1973; Dickson et al., 1996). The maximum ML density is found in winter when the ML is deepest and equals those of layers 15 and 16, but on a weekly basis the maximum ML density in area LABi equals that of layer 17. Hence the density of cLSW in the simulation ranges from $\sigma_0 = 27.77$ to 27.86 kg m^{-3} (layers 15 to 17), which corresponds well to observations and suggests that

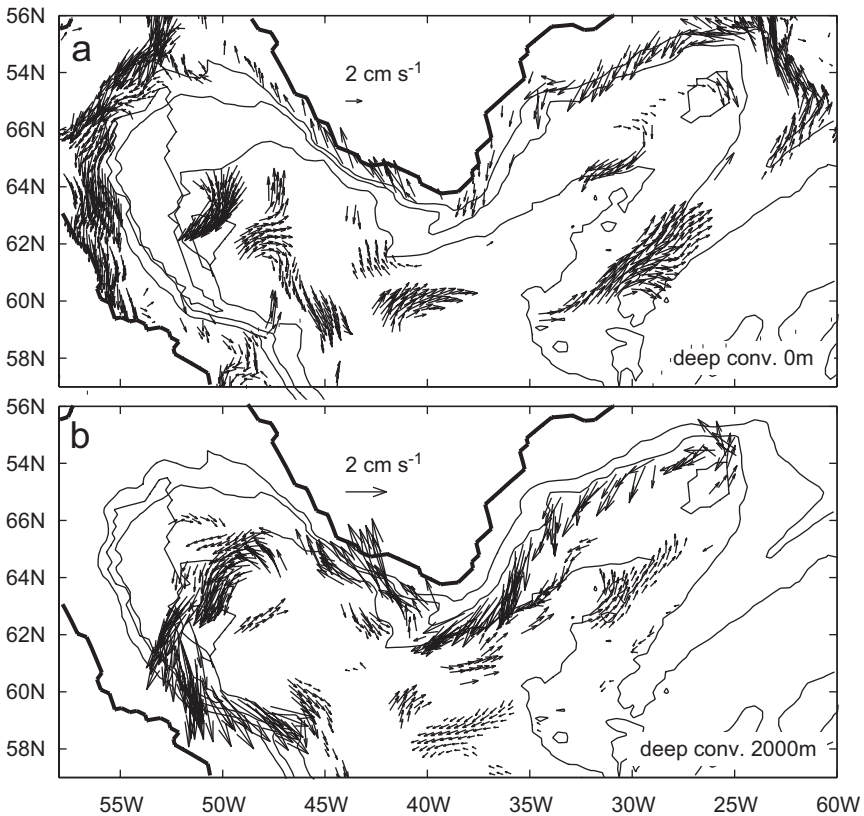

Fig. 10. Yearly anomalies of the currents at the surface (a) and at 2000 m depth (b) during the years of deep-convection in the Labrador Sea or in the Irminger Sea (which only slightly differ). Only the currents whose speed exceeds 0.9 standard deviation of the annual current speed are displayed. The thin lines indicate the location of the convection areas (Fig. 5) and the 1000, 2000, 3000, 4000 and 5000 m isobaths.

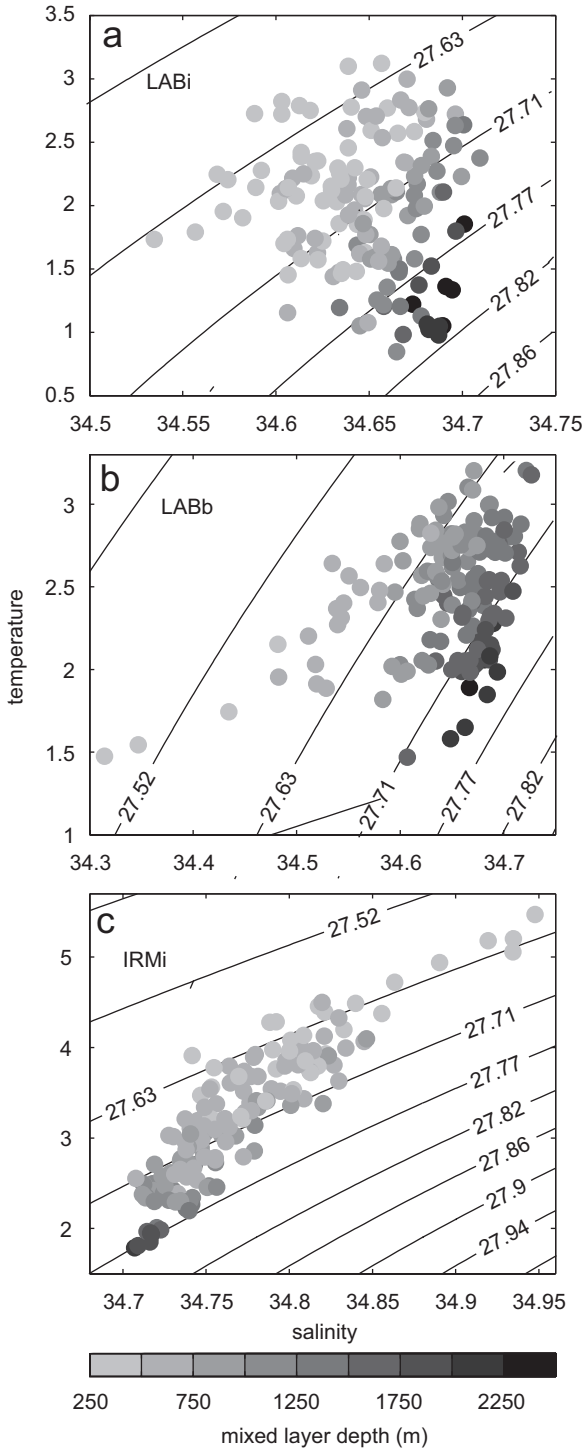

Fig. 11. Monthly averages of temperature and salinity of the ML in winter (February, March and April) in areas LABi (a), LABb (b) and IRMi (c). Shading indicates the ML depth while black lines indicate the density in σ_0 unit.

the temperature and salinity biases cancel each other. When the ML is shallow in area LABi, the temperature and salinity are similar to those in area LABb, ranging from 1.5 to 3.5 °C and from 34.5 to 34.7, respectively (Fig. 11b). In area LABb, the ML density equals those of layers 13 ($\sigma_0 = 27.63\,\mathrm{kg\,m^{-3}}$) and 14 ($\sigma_0 = 27.71\,\mathrm{kg\,m^{-3}}$), corresponding to the range of density of uLSW in the observations (Lilly et al., 1999). Hence uLSW is formed in the Labrador Current (boundary convection), where the ML is deepest, while cLSW is formed in areaLABi (interior convection), where the ML density is highest.

The winter temperature and salinity in area IRMi (Fig. 11c) suggest that the surface water masses result from horizontal mixing of two water masses of opposite characteristics, one relatively cold and fresh, the other warm and salty. This is consistent with the formation of subpolar mode water (SPMW) observed in the Irminger Sea (Pérez-Brunius et al., 2004; Lacan and Jeandel, 2004). The average characteristics of the densest ML water masses are 2 °C for temperature, 34.72 for salinity and $27.77\,\mathrm{kg\,m^{-3}}$ for potential density, which are close to the characteristics of cLSW formed in the Labrador Sea, although the latter is slightly fresher and colder. Hence these water masses will be referred to as Irminger-cLSW (I-cLSW). The lighter ML water masses have the same density as uLSW but are notably warmer and saltier, as noted by Pickart (1992), and they will be referred to as SPMW.

3.5. Formation rates

The amount of water formed in an area for a given density range can be estimated by subtracting the divergence of the isopycnal fluxes (water mass export) from the variations in volume of the layer. This includes the contribution from diapycnal mixing, which is negligible compared to convection, and does not take into account the isopycnal diffusivity, but the latter is small compared to isopycnal advection. As the changes in layer volume strongly vary on the monthly timescale, yearly averages are considered in Fig. 12.

In IRM box (see Fig. 2), the calculation is done for layers 15 and 16, which covers the range of density of the I-cLSW. At the beginning of the simulation when the convective mixing is weak, the rate of formation (or the diapycnal flux) is almost constant at about 2.7 Sv (gray line, Fig. 12a),

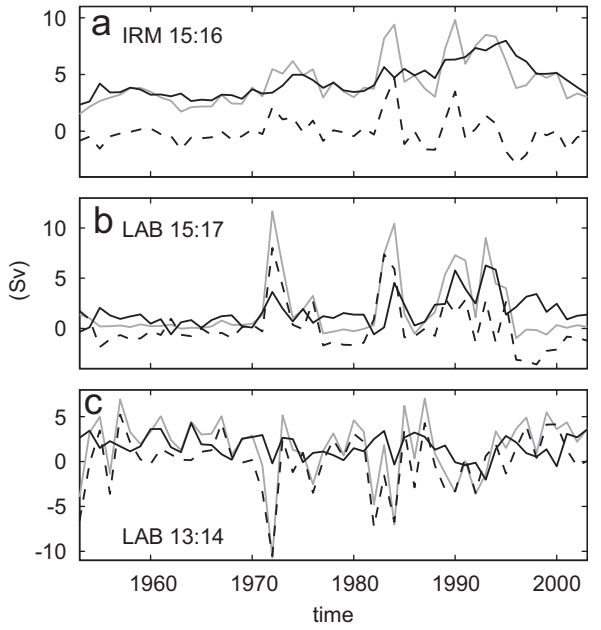

Fig. 12. Flux representing the creation of mass (gray line), divergence of the isopycnal fluxes (black thin line) and changes in volume (black dashed line) of layers 15–16 in the Irminger Sea (a), and 15–17 (b) and 13–14 (c) in the Labrador Sea.

indicating that I-cLSW is formed every winter. The diapycnal fluxes then increase, peaking in the mid-1970s, the mid-1980s, and the early 1990s, when convection is deep, so that the overall average rate of formation of I-cLSW is 4.3 Sv. Fig. 12a shows that the formation rate is of the same amplitude as the divergence of the isopycnal fluxes (thin line), while the variations in volume (dashed line) are well correlated with the diapycnal fluxes but remain much smaller. This suggests that I-cLSW is rapidly exported out of the Irminger Sea, which may be partly due to the close proximity of area IRMi to the boundary currents. The formation rate of lighter SPMW in the Irminger Sea averages 8.1 Sv, and is well correlated with that of I-cLSW ($r = 0.69$). These water masses are also rapidly exported out of the basin. As the amount of SPMW formed in the Irminger Sea has not been quantified in observations (Hanawa and Talley, 2001), we do not know if these formation rates are realistic. However, because of the proximity of the boundary current, it is likely that the newly formed water is expelled too rapidly out of the Irminger Sea.

The situation is different in the Labrador Sea. In LAB box (see Fig. 2), the formation rate of cLSW is very small (1.7 Sv in overall average), except for peaks reaching 7–12 Sv when the convection is deep (Fig. 12b). During deep convection events, the rate of formation of cLSW averages 8.3 Sv, which corresponds well to the 6.4–8.5 Sv estimates of Rhein et al. (2002) for the formation of cLSW during high NAO phases (from 1988 to 1994). The formation rate and the variations in volume are of the same order of magnitude and highly correlated ($r = 0.86$), while the divergence of the isopycnal fluxes is a bit smaller and less correlated. This suggests that the Labrador Sea primarily acts as a reservoir for the newly formed cLSW, with limited export out of the basin.

The production of uLSW is minimum when cLSW is formed and maximum when convection is only shallow, as peaks of negative diapycnal fluxes for uLSW coincide with positive ones for cLSW, and the formation rates of uLSW and cLSW are negatively correlated ($r = -0.6$ at 0 lag, Fig. 12c). This is consistent with the findings of Kieke et al. (2006) who estimated the formation rates of uLSW and cLSW in the subpolar North Atlantic from CFC-11 data. In the simulation, the production of uLSW averages to 1.7 Sv for the whole period, and to 2.7 Sv from 1953 to 1970, when it is largest. From 1970 to 1997, when the formation of cLSW is largest, the production of uLSW averages 0.64 Sv, which is notably lower than the 3.2–3.3 Sv estimate of Kieke et al. (2006) during that period. However, the authors suggest that this estimate includes uLSW formed in the Irminger Sea, which is not taken into account in the simulation.

4. Export of the newly formed water masses

4.1. Irminger Sea

As noted above, the water masses formed in the Irminger Sea are rapidly exported out of the basin. This is clearly seen in the evolution of the potential vorticity of I-cLSW in the deep convection composite (Fig. 13). Note that the model is formulated to conserve potential vorticity on each isopycnal (Bleck et al., 1992), meaning that it is a particularly valuable tracer for diagnosing the pathway and timescale of the export of the newly-formed water masses. In winter, there is a potential vorticity minimum in the northern part of the Irminger Sea, where the area IRMi was identified, and another smaller one in the southern part of the basin, indicating that the formation of I-cLSW may also happen there, as in the observations (Pickart et al.,

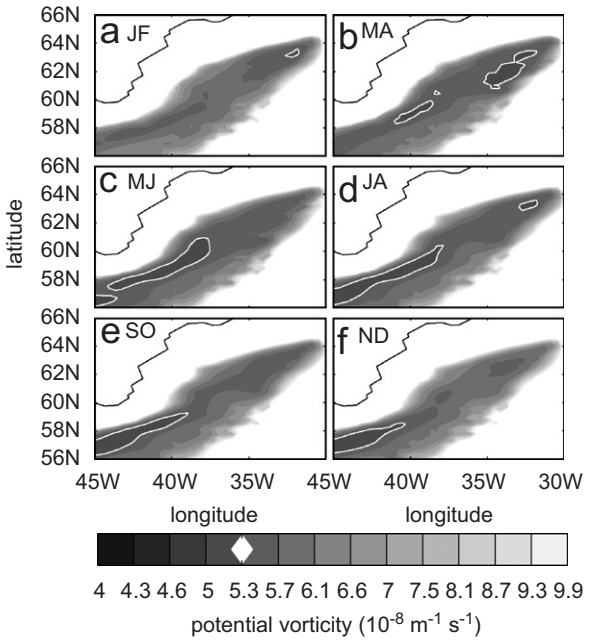

Fig. 13. Composite of the potential vorticity of layers 15 and 16 during years with deep convection in the Irminger Sea in January–February (JF), March–April (MA), May–June (MJ), July–August (JA), September–October (SO) and November–December (ND). The white lines show potential vorticity smaller than $5.3 \times 10^{-8}\,m^{-1}\,s^{-1}$.

2003; Bacon et al., 2003). By May–June, the two potential vorticity minima have merged and propagated southwestward, while another minimum of potential vorticity emerges from the Labrador Sea. The latter seems to reflect the formation of cLSW in LABi which is advected by the northeastward flow that goes from the Labrador Sea to the Irminger Sea (Fig. 2, see below). In summer (July–August), the potential vorticity minimum in the Irminger Sea has moved further southwestward and cannot be distinguished any more from that coming from the Labrador Sea, presumably because of isopycnal mixing of potential vorticity due to isopycnal diffusivity of the layer thickness. From September to December, the potential vorticity minimum propagates further to the southwest. Note that the minimum of potential vorticity that is seen in the northern Irminger Sea during summer is not related to deep water formation, but seems to be associated with a seasonal contraction of the gyre circulation during summer (not shown).

To further trace the path of the newly formed water in the Irminger Sea, we consider the salinity and transport of LSW along sections A25 and AR7W. For section A25, we integrate the transport and average the salinity in the southward jet, i.e., from the coast to 40°W. For section AR7W in the Labrador Sea, we consider separately the northwestward branch of the cyclonic gyre, from 57°N to the northern coast, and its southeastward branch, from the southern coast to 57°N. Note that we do not distinguish the transport due to the export of the newly formed deep water from the recirculation of deep water associated with the wind-driven subpolar gyre circulation. As we are interested in correlations on the seasonal timescale, we removed a linear trend from the salinity and the transport which reflect low-frequency changes and/or simulation drift. The overall trend is of the order of 0.12 Sv/yr (0.24 Sv/yr) for the transport across section A25 (respectively, AR7W), due to the intensification of the subpolar gyre from 1950s to 1990s (not shown) which is consistent with observations (Belkin, 2004). It ranges from $-1.6 \times 10^{-3}\,yr^{-1}$ to $-2.4 \times 10^{-3}\,yr^{-1}$ for the salinity, consistent with observations (Curry and Mauritzen, 2005).

Fig. 14, which shows the correlation with the index of convection in IRMi (defined as the anomalies of the ML volume in February, March and April in IRMi as in Fig. 9), mostly exhibits the annual modulation of the correlations due to the autocorrelation of the transport and salinity anomalies. Nonetheless, the correlation with salinity anomalies along section A25 peaks when convection leads by 2 months (panel b, solid line), consistent with the propagation of potential vorticity in Fig. 13. The correlation is positive, indicating that I-cLSW is relatively salty, which is consistent with the characteristics of I-cLSW (Fig. 11). The correlation is also positive with the transport anomalies across section A25 (panel a, solid line), as expected from Fig. 10. The time series remain correlated in the Labrador Sea section further downstream (dashed and dash-dotted lines), albeit to a lesser extent as there is mixing with cLSW formed in LABi, and at increasing lag. Note that the correlation with the transport anomalies in section AR7W peaks at lags somewhat smaller than with the salinity anomalies, suggesting that fast topographic waves precede the advection of the newly formed water masses (see also Section 4.3). The correlation is also positive at negative lags (when convection lags), indicating a complex coupling between the hydrography, circulation at depth and convection.

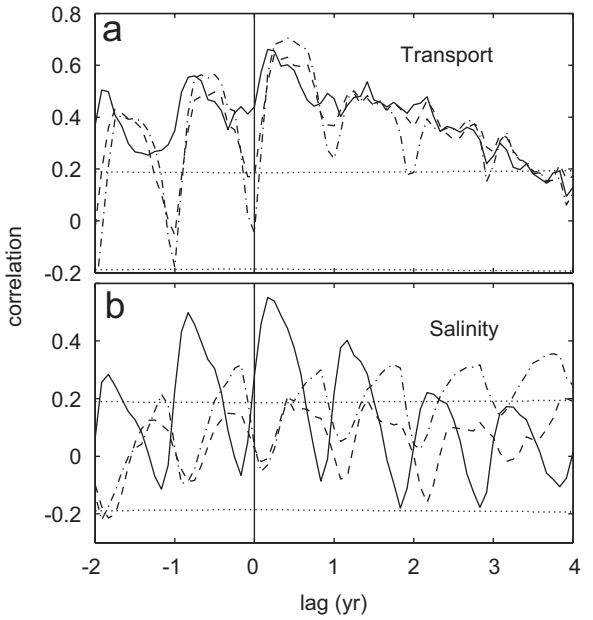

Fig. 14. Correlation of the Irminger Sea convection index in winter with anomalies of the isopycnal transport (a) across and salinity (b) along sections A25 (solid lines), AR7W-north (dashed lines) and AR7W-south (dash-dotted lines). The anomalies of the isopycnal transport and salinity are calculated for layer 15. The dotted lines represent the estimated 5% significance level. Convection in IRMi leads for positive lags.

4.2. Labrador Sea

Based on the composite of deep convection in the Labrador Sea, cLSW is formed in February–April in the center of the basin as indicated by the minimum of potential vorticity in Fig. 15a. Note that there is no potential vorticity minimum in the northern Irminger Sea, because the years of convection in LABi slightly differ from or precede the years of convection in IRMi (Section 3), and because we are considering an additional deeper layer (layer 17) here. In summer, the region where the potential vorticity is minimum widens in the interior of the Labrador Sea, and two extensions appear, one in the Labrador Current and the other toward the Irminger Sea. In the winter of the year following convection (yr + 1), the extension in the Labrador Current has propagated as far as Flemish Cap, and during summer it keeps propagating eastward. The potential vorticity extension toward the Irminger Sea seems to slowly propagate northeastward, but the signal is not clear as the potential vorticity of cLSW is higher in the Irminger Sea (Fig. 13). Note that the potential vorticity remains low in the interior of the Labrador Sea because of the permanent doming of the isopycnals that is associated with the cyclonic gyre circulation.

The normalized anomalies of the winter ML volume in LABi are used as an index of convection in the Labrador Sea. The salinity anomalies along the northern part of section AR7W are negatively correlated with convection in LABi, suggesting that the cLSW formed in LABi is relatively fresh, but the correlation is only significant when convection leads the salinity anomalies by 2 years (gray plain line in Fig.16). Along the southern part of the section, the correlation with the salinity anomalies is still negative, but it is not significant (gray dashed lines). The correlation between convection in LABi and the transport anomalies across section AR7W is important a few months after convection in LABi but maximum 18 months after convection (black solid and dashed lines). This confirms that the newly formed water masses in part accumulate and recirculate in the interior of the Labrador Sea. The correlations at negative lags (when convection lags) are much less significant, except for the transport across the southern part of section AR7W, presumably reflecting the faster barotropic response to the NAO.

During the composite event of shallow convection in the Labrador Sea, uLSW is formed in area LABb. The potential vorticity of uLSW is, indeed, minimum along the continental slope in the northwest of the Labrador Sea in winter (Fig. 17). Note that the potential vorticity is always maximum in the center of the Labrador and Irminger Seas because of the permanent doming of the cLSW below. Three months later, the minimum of potential vorticity is located seaward of the Hamilton Bank. The southward propagation continues until Flemish Cap, which is reached less than 6 months after convection. Throughout the year, potential vorticity is also minimum seaward of Flemish Cap, because of the convergence of the Gulf Stream and the Labrador Current. However, the eastern tip of the minimum only migrates eastward in November–December–January following the composite event of convection, which is presumably due to the arrival of the newly-formed uLSW water masses. Some formation of uLSW seems to happen also offshore of the southeastern tip of Greenland, as indicated by a local minimum of potential vorticity in winter. This minimum propagates around the Labrador Sea and reaches area LABb in approximately 1 year.

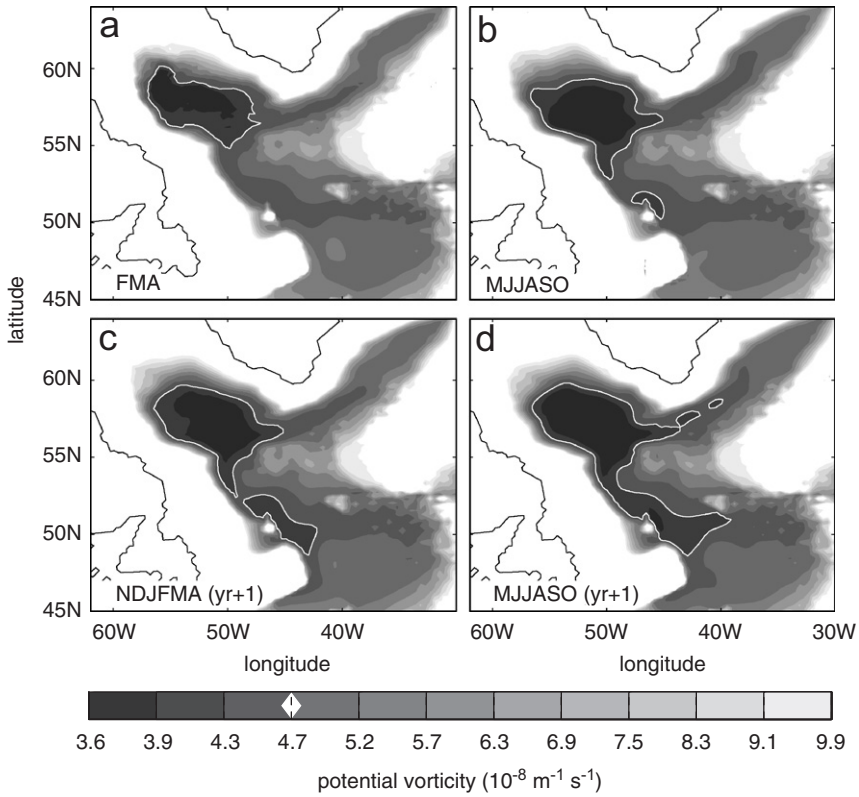

Fig. 15. Composite of the potential vorticity of layers 15–17 during deep convection in the Labrador Sea, in February–April (FMA) and in the following 6-months: May–October (MJJASO), November–April (NDJFMA, year+1), May–October (MJJASO, year+1). The white lines show potential vorticity smaller than $4.7 \times 10^{-8}\ m^{-1}\ s^{-1}$.

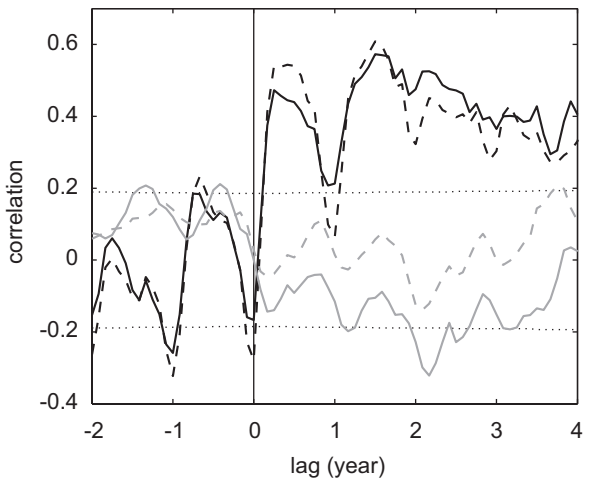

Fig. 16. Same as Fig. 14 for convection in LABi and anomalies of the isopycnal transport (black lines) across and salinity (gray lines) along sections AR7W-north (solid line) and AR7W-south (dashed line). The anomalies of the isopycnal transport and salinity are calculated for layers 15–17. Convection in LABi leads for positive lags.

4.3. Variability of the DWBC

In the simulation, we monitor the DWBC upstream of Flemish Cap, in order to avoid the influence of the North Atlantic Current (see section DWBC, Fig. 2). The Labrador Current is composed of one branch above the continental shelf and another above the continental slope centered around 50.5°W (Fig. 18a), as described by Lazier and Wright (1993). The current speed in the two branches is maximum at the surface, but the southward transport is maximum for LSW and takes place over the continental slope (colors in Fig. 18b). A counter-current is seen seaward of the Labrador Current, as in the observations (Fischer et al., 2004), reflecting a recirculation which goes back to the interior of the Labrador Sea. Hence the transport of LSW in the DWBC (24.1 Sv on average) consists of the wind-driven gyre circulation (8.3 Sv, given by the recirculation) plus the net throughput of LSW formed in the subpolar gyre

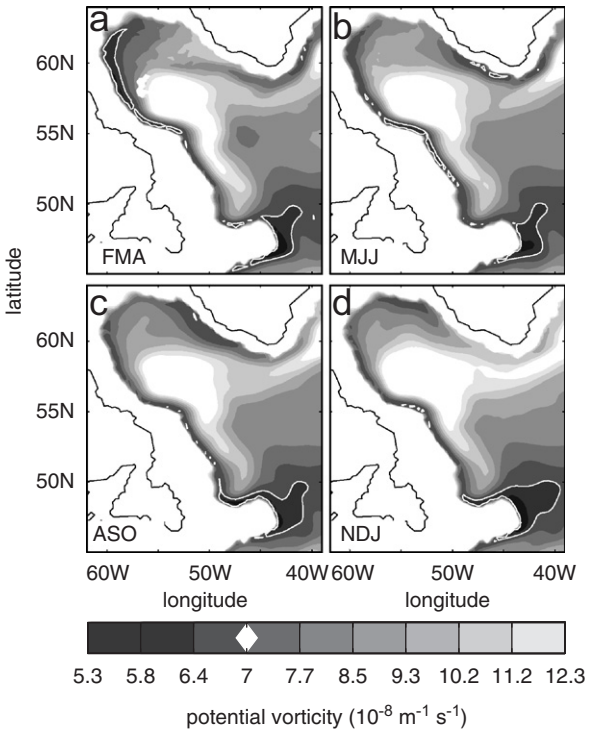

Fig. 17. Composite of the potential vorticity of layers 13 and 14 during shallow convection in the Labrador Sea, in February–April (FMA), May–July (MJJ), August-October (ASO) and November–January (NDJ, year+1). The white lines show potential vorticity smaller than $7 \times 10^{-8}\,m^{-1}\,s^{-1}$.

(15.8 Sv). The latter approximately equals the average rate of formation of LSW (7.7 Sv) and SPMW (8.1 Sv) in the Labrador and Irminger Seas (see Section 3).

The transport of dense water across section DWBC compares reasonably well with the observations of Fischer et al. (2004) for the period 1996–2001. In the simulation, the transport of cLSW during that period is 9.2 Sv, slightly less than the observed 11.4 Sv, while the transport of uLSW is 17.7 Sv, larger than the observed 13.5 Sv. However, the transport of water denser than $\sigma_0 = 27.86\,kg\,m^{-3}$, which mostly comes from the Denmark Strait overflow (but is also formed by convection in the Labrador Sea), is 0.8 Sv, hence far less than the observed 3.4 Sv (for $\sigma_0 = 27.88\,kg\,m^{-3}$). Because of this model flaw, the simulated DWBC is not affected by the northern boundary conditions of the regional simulation. At the location of the DWBC section, it should also be little influenced by the subtropical gyre circulation, and thus by the southern boundary condition.

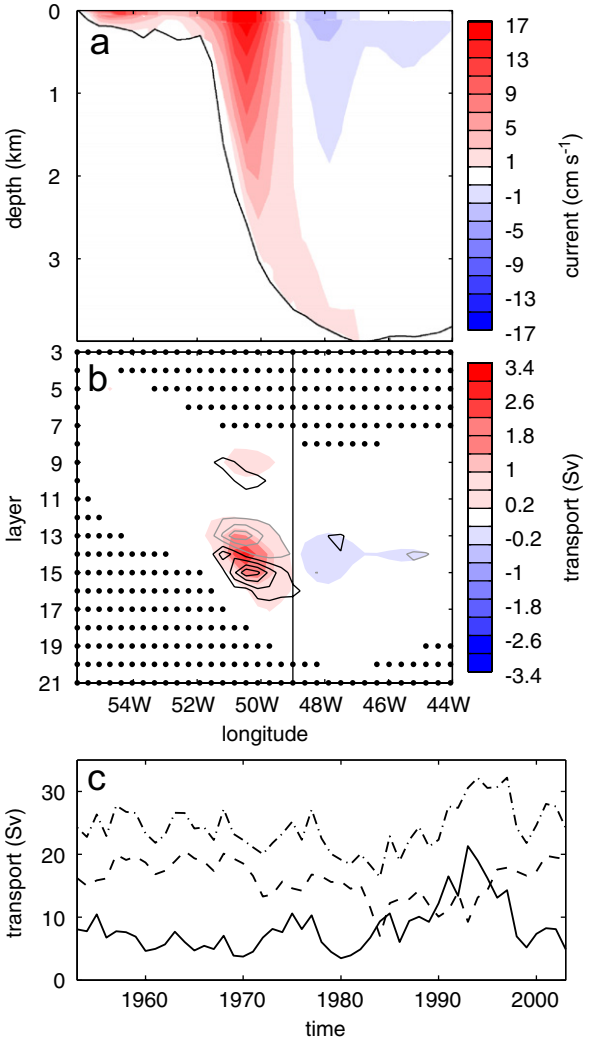

Fig. 18. (a) Mean current (positive southwestward) normal to section DWBC, (b) mean isopycnal transport across section DWBC, and the first EOF calculated from yearly averages (black for positive, gray for negative, 0.2 Sv interval contoured around 0). The black dots identify grid points where the layer vanishes, after integration of the transport in the mixed layer to the layer of corresponding density at depth. The vertical line indicates the eastern limit for integrating the southward transport, whose time series are given (c) for layers 13–14 (uLSW, dashed line), 15–17 (cLSW, plain line) and 13–17 (LSW, dash-dotted line).

A principal component analysis reveals that the first mode of variability of the transport across section DWBC (explaining 47% of the variance) consists of a decrease of the southward jet in uLSW and an increase of the southward jet in cLSW, or vice-versa (contours in Fig. 18b). When integrating the southward transport from the boundary to 49°W (black vertical line in Fig. 18b), we observe indeed that the transport of uLSW is anti-correlated

with that in cLSW (Fig. 18c), the anti-correlation being maximum when the transport of uLSW leads that of cLSW by 2 years ($r = -0.62$). This lag is consistent with uLSW being rapidly exported out of the Labrador Sea while cLSW is more slowly exported.

The correlation of the anomalies of the DWBC transport with convection in areas LABi and IRMi gives consistent results (Fig. 19). The uLSW transport anomalies are negatively correlated with convection in LABi and IRMi as the formation of uLSW is maximum when convection is shallow. The correlation is minimum when convection leads by a few months, but also significant when convection lags the DWBC transport, presumably because of the preconditioning. The cLSW transport anomalies are positively correlated with convection in IRMi and LABi, and maximum for convection in IRMi when the latter leads by a few months ($r = 0.65$). This lag approximately corresponds to the lag between convection in IRMi and the cLSW transport anomalies across section AR7W-south, which is close to section DWBC (Fig. 14), and is less than the advection time from the Irminger Sea to section DWBC. This suggests that the advection of the newly formed water masses is preceded by a faster wave propagation. The phase speed is of the order of $30\,\mathrm{cm\,s^{-1}}$ ($30\,\mathrm{km\,day^{-1}}$). This is larger than the phase speed of topographic Rossby waves observed downstream in the DWBC, which is of the order of $3-10\,\mathrm{km\,day^{-1}}$ (Pickart and Watts, 1990), but smaller than the theoretical phase speed of baroclinic Kelvin waves. However, our estimate seems consistent with the slower propagation speed of Kelvin waves seen in numerical models of limited resolution (Hsieh et al., 1983).

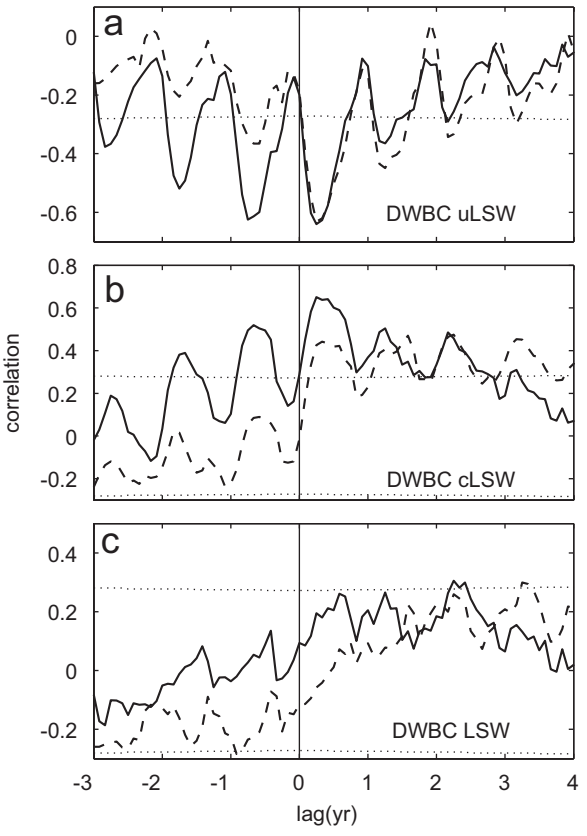

Fig. 19. Correlation of convection in IRMi (solid lines) and in LABi (dashed lines) with the anomalies of the isopycnal transport across section DWBC for layers (a) 13–14 (uLSW), (b) 15–17 (cLSW) and (c) 13–17 (LSW). A linear trend was removed from the transport in the DWBC. The dotted lines represent the estimated 5% significance level. Convection leads for positive lags.

The correlation of the DWBC transport with convection in LABi is less than ($r \leqslant 0.5$) that with convection in IRMi, but it hardly decreases with lag until convection leads by more than 5 years, except for the annual modulation. This confirms that cLSW formed in the Labrador Sea accumulates and recirculates in the basin, and is only slowly exported out of the Labrador Sea. Besides, the accumulation of cLSW in the Labrador Sea acts as an integrator for the time series of convection in LABi, reducing its correlation with the DWBC transport anomalies. Finally the correlation of the LSW (uLSW + cLSW) transport anomalies with convection in the Irminger Sea or in the Labrador Sea is hardly significant, and less than that obtained when we only consider cLSW, with somewhat longer time lags. This occurs because uLSW and cLSW compensate each other in the DWBC transport. Note that the annual modulation of the correlation with LSW transport anomalies is reduced because the respective influence of convection in LABi and IRMi on the cLSW transport anomalies are slightly out of phase.

5. Conclusions

A hind cast simulation of the North Atlantic circulation is used to investigate the formation and export of deep water out of the subpolar gyre from 1953 to 2003. Deep water formation primarily occurs at three sites: in the Irminger Sea, in the Labrador Sea interior and in the Labrador Current.

In the Irminger Sea, cLSW is formed when the surface currents are intense. The newly formed

water masses are advected by the East Greenland current to the Labrador Sea, and through the Labrador Sea to the Labrador Current. The speed of these currents increases when deep water is formed in the Irminger Sea because of a concurrent intensification of the subpolar gyre, which might be due to the atmospheric thermohaline forcing (Häkkinen and Rhines, 2004). This results in the acceleration of the export of the cLSW newly formed in the Irminger Sea, which reaches Flemish Cap in less than one year. The advection of the newly formed cLSW is preceded by the fast propagation of waves, which reach Flemish Cap only a few months after convection occurred in the Irminger Sea.

Each winter, the ML deepens in the Labrador Current, producing uLSW. When the atmospheric buoyancy forcing is intense, the area where the ML deepens extends to the interior of the Labrador Sea where the surface density is higher, so that cLSW is formed. The production of uLSW is minimum when the convection is deep in the interior since more uLSW is converted into cLSW. This mechanism is consistent with observations (Stramma et al., 2004; Kieke et al., 2006). However, it is important to notice that in the simulation, convection is deepest in the Labrador Current while it is sporadic in the interior of the Labrador Sea. In reality the deepest overturning occurs in the interior of the Labrador Sea, and boundary convection is more sporadic. This suggests that convection in the Labrador Current is overestimated in the simulation, even though the rate of formation of uLSW is underestimated.

While uLSW is advected out of the Labrador Sea in few months as it is formed in the intense boundary current, cLSW tends to accumulate and recirculate in the interior, with a residence time of a few years, hence only slowly exiting the Labrador Sea. In an eddy-resolving model, the export of water masses newly formed in the interior of a convective basin is achieved by turbulent fluxes to the surrounding boundary current (Spall, 2004). This involves spatial scales of the order of the Rossby deformation radius, which are not resolved by the model. Nevertheless, the "reservoir effect" in the Labrador Sea described in the simulation is realistic: Straneo et al. (2003) estimated a 4 year residence time of LSW in the interior of the Labrador Sea from an advective–diffusive model based on observations at 700 m depth (Lavender et al., 2000). The same residence time was obtained by Kvaleberg and Haine (2006) from a similar method based on the circulation fields of Faure and Speer (2005). Note that these studies are based on mean circulation fields, while our study suggests an increase of 20–40% of the boundary currents during cLSW formation in the interior of the Labrador Sea, suggesting that the residence time of LSW in the above studies is overestimated.

In the DWBC, the transports of uLSW and cLSW are highly anti-correlated. This compensating mode is the first mode of variability of the DWBC transport, and it results in the reduction of the variability of the net transport of LSW compared to the variability of deep water formation. This mechanism has been suggested in observations (Schott et al., 2006) and may explain why the net DWBC transport is not directly linked to the history of deep water formation in the Labrador Sea. Nevertheless, the transport of uLSW in the DWBC is overestimated in the simulation, albeit with a too small rate of formation of uLSW in the Labrador Sea, hence presumably because of an overestimated rate of formation of SPMW in the Irminger Sea.

Since convection in the Irminger and Labrador Seas often occur simultaneously, their influence on the DWBC tends to be somewhat mixed. Still, the cLSW transport anomalies are mostly correlated with convection in the Irminger Sea, which leads them by a few months, while it is less correlated with convection in the Labrador Sea, which leads them by 1–4 years. This suggests that the influence of deep water formation on the DWBC transport depends on the location of convection, although the export of I-cLSW may be too fast in the simulation. Indeed, convection in the Irminger Sea mostly occurs in the northwestern part of the basin, near the fast boundary currents, while it has been observed in the southern interior of the basin, forced by the Greenland tip jet (Pickart et al., 2003). Such a small scale atmospheric feature is not present in the NCEP/NCAR reanalysis fields used to force the model. Moreover, the absence of eddies in the simulation impedes the salty water masses carried by the East Greenland Current from spreading in the interior, which should facilitate convection. Nevertheless, the characteristics of the water masses formed by convection in the northern Irminger Sea are consistent with the formation of SPMW described in observations (Pérez-Brunius et al., 2004; Lacan and Jeandel, 2004), resulting from mixing of subtropical and subarctic water masses.

Finally, a word of caution is needed. The transport of dense water across the Greenland–Scotland Ridge is much weaker than in observations where, in the DWBC, the transport of dense water formed in the Nordic Seas equals, on average, that of cLSW (Fischer et al., 2004). Therefore it may have a considerable influence on the DWBC variability which is not represented in the model, although the variability in the volume transport across the Greenland–Scotland Ridge is poorly known (Curry and Mauritzen, 2005). Moreover, the export of deep water formed in the Nordic Seas may have an influence on the recirculation patterns in the Labrador and Irminger Seas (Käse et al., 2001).

Acknowledgments

We are thankful to A.-B. Sandø and Y. Gao for providing the data of the simulation, which were supported by the Research Council of Norway through the NOCLIM and NOTUR programs (HD), and to the two anonymous reviewers for very constructive comments. Support from the European FP6 project DYNAMITE (Contract 003903-GOCE) and the Institut Universitaire de France (to CF) is gratefully acknowledged.

References

Bacon, S., Gould, W.J., Jia, Y., 2003. Open-ocean convection in the Irminger Sea. Geophysical Research Letters 30 [doi:10.1029/2002GL016271].

Belkin, I.M., 2004. Propagation of the "Great Salinity Anomaly" of the 1990s around the northern North Atlantic. Geophysical Research Letters 31 [doi:10.1029/2003GL19334].

Bentsen, M., Drange, H., 2000. Parameterizing surface fluxes in ocean models using the NCEP/NCAR reanalysis data. In: RegClim General Technical Report 4. Norwegian Institute for Air Research, Kjeller, Norway, pp. 149–158.

Bentsen, M., Drange, H., Furevik, T., Zhou, T., 2004. Simulated variability of the Atlantic meridional overturning circulation. Climate Dynamics 22, 701–720.

Bleck, R., Rooth, C., Hu, D., Smith, L.T., 1992. Salinity-driven thermocline transients in a wind- and thermohaline-forced isopycnic coordinate model of the North Atlantic. Journal of Physical Oceanography 22, 1486–1505.

Bower, A.S., Hunt, H.D., 2000. Lagrangian observations of the deep western boundary current in the North Atlantic ocean. Part 2: the Gulf Stream–DWBC crossover. Journal of Physical Oceanography 30, 784–804.

Bretherton, C.S., Widmann, M., Dymnikov, V.P., Wallace, J.M., Bladé, I., 1999. The effective number of spatial degrees of freedom of a time-varying field. Journal of Climate 12, 1990–2009.

Cunningham, S.A., Haine, T.W.N., 1995. Labrador Sea Water in the eastern North Atlantic. Part 1: a synoptic circulation inferred from a minimum in potential vorticity. Journal of Physical Oceanography 25, 649–665.

Cuny, J., Rhines, P.B., Niiler, P.P., Bacon, S., 2002. Labrador Sea boundary currents and the fate of the Irminger Sea Water. Journal of Physical Oceanography 32, 627–647.

Cuny, J., Rhines, P.B., Lazier, J., 2005. Convection above the Labrador continental slope. Journal of Physical Oceanography 35, 489–511.

Curry R.G., 2006. Hydrobase 2, ⟨http://www.whoi.edu/science/PO/hydrobase⟩, Woods Hole Oceanographic Institution.

Curry, R.G., Mauritzen, C., 2005. Dilution of the northern North Atlantic ocean in recent decades. Science 308, 1772–1774.

Dickson, R.R., Brown, J., 1994. The production of North Atlantic Deep Water: sources, rates and pathways. Journal of Geophysical Research 99, 12.319–12.341.

Dickson, R.R., Lazier, J., Meincke, J., 1996. Long term coordinated changes in the convection activity of the North Atlantic. Progress in Oceanography 38, 241–295.

Drange, H., Simonsen, K., 1996. Formulation of air–sea fluxes in the ESOP2 version of MICOM. Technical Report 125, Nansen Environmental and Remote Sensing Center, Bergen, Norway, 23pp.

Drange, H., Gerdes, R., Gao, Y., Karcher, M., Kauker, F., Bentsen, M., 2005. Ocean general circulation modelling of the Nordic Seas. In: Drange, H., Dokken, T.M., Furevik, T., Gerdes, R., Berger, W. (Eds.), The Nordic Seas: An Integrated Perspective, vol. 158. American Geophysical Union.

Eden, C., Willebrand, J., 2001. Mechanism of interannual to decadal variability of the North Atlantic Circulation. Journal of Climate 14, 2266–2280.

Eldevik, T., 2002. On frontal dynamics in two model oceans. Journal of Physical Oceanography 32, 2915–2925.

Faure, V., Speer, K., 2005. Labrador Sea Water circulation in the northern North Atlantic Ocean. Deep-Sea Research 2 (52), 565–581.

Fischer, J., Schott, F., 2002. Labrador Sea Water tracked by profiling floats—from the boundary current into the open North Atlantic. Journal of Physical Oceanography 32, 573–584.

Fischer, J., Schott, F.A., Dengler, M., 2004. Boundary circulation at the exit of the Labrador Sea. Journal of Physical Oceanography 34, 1548–1570.

Friedrich, H., Levitus, S., 1972. An approximation to the equation of state for sea water, suitable for numerical ocean models. Journal of Physical Oceanography 2, 514–517.

Häkkinen, S., Rhines, P.B., 2004. Decline of subpolar North Atlantic Circulation during the 1990s. Science 304, 555–559.

Hanawa K., Talley, L.D., 2001. Mode waters. In: Siedler, G., Church, J., Gould, J., (Eds.), Ocean Circulation and Climate: Observing and Modelling the Global Ocean. Academic Press, New York, pp. 373–386.

Harder, M., 1996. Dynamik, rauhigkeit und alter des meereises in der Arktis. Ph.D. Thesis, Alfred-Wegener-Institut für Polar- und Meeresforschung, Bremerhaven, Germany, pp. 124.

Hátún, H., Sandø, A.B., Drange, H., Hansen, B., Valdimarsson, H., 2005a. Influence of the Atlantic Subpolar Gyre on the Thermohaline Circulation. Science 309, 1841–1844.

Hátún, H., Sandø, A.B., Drange, H., Bentsen, M., 2005b. Seasonal to decadal temperature variations in the

Faroe–Shetland inflow waters. In: Drange, H., Dokken, T.M., Furevik, T., Gerdes, R., Berger, W. (Eds.), The Nordic Seas: An Integrated Perspective, vol. 158. American Geophysical Union, pp. 239–250.

Hsieh, W.W., Davey, M.K., Wajsowicz, R.C., 1983. The free Kelvin wave in finite-difference numerical models. Journal of Physical Oceanography 13, 1383–1397.

Hurrell, J.W., 1995. Decadal trends in the North Atlantic Oscillation: regional temperatures and precipitation. Science 269, 676–679.

Käse, R.H., Biastoch, A., Stammer, D.B., 2001. On the mid-depth circulation in the Labrador and Irminger Seas. Geophysical Research Letters 28 [doi:10.1029 /2001GL013192].

Kieke, D., Rhein, M., Stramma, L., Smethie, W.M., LeBel, D.A., Zenk, W., 2006. Changes in the CFC inventories and formation rates of Upper Labrador Sea Water, 1997–2001. Journal of Physical Oceanography 36, 64–86.

Krauss, W., 1995. Currents and mixing in the Irminger Sea and in the Iceland basin. Journal of Geophysical Research 100, 10851–10871.

Kvaleberg, E., Haine, T.W.N., 2006. Labrador Sea Water transport rates and pathways in the subpolar North Atlantic Ocean. ASOF Newsletter 5, 25–27.

Lacan, F., Jeandel, C., 2004. Subpolar Mode Water formation traced by neodynium isotopic composition. Geophysical Research Letters 31 [doi:10.1029/2004GL019747].

Lavender, K.L., Davis, R.E., Owens, W.B., 2000. Mid-depth recirculation observed in the interior Labrador and Irminger Seas by direct velocity measurements. Nature 407, 66–69.

Lazier, J.R.N., 1973. The renewal of Labrador Sea Water. Deep-Sea Research 20, 341–353.

Lazier, J.R.N., 1980. Oceanographic conditions at Ocean Weather Ship Bravo, 1964–1974. Atmosphere–Ocean 18, 227–238.

Lazier, J.R.N., 1995. The salinity decrease in the Labrador Sea over the past thirty years. In: Martinson, D.G., et al. (Eds.), Natural Climate Variability on Decade-to-Century Time Scales. National Research Council, pp. 295–304.

Lazier, J.R.N., Wright, D.G., 1993. Annual velocity variations in the Labrador Current. Journal of Physical Oceanography 23, 659–678.

Lazier, J.R.N., Hendry, R., Clarke, R.A., Yashayaev, I., Rhines, P., 2002. Convection and restratification in the Labrador Sea, 1990–2000. Deep-Sea Research 1 (49), 1819–1835.

Levitus, S., Boyer, T.P., 1994. World Ocean Atlas 1994 Volume 4: Temperature. NOAA Atlas NESDIS 4.

Levitus, S., Burgett, R., Boyer, T.P., 1994. World Ocean Atlas 1994 Volume 3: Salinity. NOAA Atlas NESDIS 3.

Lilly, J.M., Rhines, P.B., Visbeck, M., Davis, R., Lazier, J., Schott, F., Farmer, D., 1999. Observing deep convection in the Labrador Sea during winter 94/95. Journal of Physical Oceanography 29, 2065–2098.

Manabe, S., Stouffer, R.J., 1995. Simulation of abrupt climate change induced by freshwater input to the North Atlantic Ocean. Nature 378, 165–167.

Marshall, J., Schott, F.A., 1999. Open ocean convection: observations, theory and models. Reviews of Geophysics 37, 1–64.

Marshall, J., Johnson, H., Goodman, J., 2001. A study of the interaction of the North Atlantic Oscillation with ocean circulation. Journal of Climate 14, 1399–1421.

Mauritzen, C., Häkkinen, S., 1999. On the relationship between dense water formation and the "meridional overturning cell" in the North Atlantic Ocean. Deep-Sea Research I 46, 877–894.

Mignot, J., Frankignoul, C., 2005. On the variability of the Atlantic meridional overturning circulation, the North Atlantic Oscillation and the El Niño-southern oscillation in the Bergen Climate Model. Journal of Climate 18, 2361–2375.

Paillet, J., Arhan, M., McCartney, M.S., 1998. Spreading of Labrador Sea Water in the eastern North Atlantic. Journal of Geophysical Research 103, 10223–10239.

Pérez-Brunius, P., Rossby, T., Watts, D.R., 2004. Transformation of the warm waters of the North Atlantic from a geostrophic streamfunction perspective. Journal of Physical Oceanography 34, 2238–2256.

Pickart, R.S., 1992. Water mass components of the North Atlantic deep western boundary current. Deep-Sea Research 39, 1553–1572.

Pickart, R.S., Torres, D.J., 2002. Hydrography of the Labrador Sea during active convection. Journal of Physical Oceanography 32, 428–457.

Pickart, R.S., Watts, D.R., 1990. Deep western boundary current variability at Cape Hatteras. Journal of Marine Research 48, 765–791.

Pickart, R.S., Spall, M.A., Lazier, J., 1997. Mid-depth ventilation in the western boundary current system of the subpolar gyre. Deep-Sea Research I 44, 1025–1054.

Pickart, R.S., Straneo, F., Moore, G.W.K., 2003. Is Labrador Sea Water formed in the Irminger basin? Deep-Sea Research I 50, 23–52.

Reverdin, G., Niiler, P.P., Valdimarsson, H., 2003. North Atlantic ocean surface currents. Journal of Geophysical Research 108 [doi:10.1029/2001JC001020].

Rhein, M., Fischer, J., Smethie, W.M., Smythe-Wright, D., Weiss, R.F., Mertens, C., Min, D.-H., Fleischmann, U., Putzka, A., 2002. Labrador Sea Water: pathways, CFC inventory and formation rates. Journal of Physical Oceanography 32, 648–665.

Schott, F., Zantopp, R., Stramma, L., Dengler, M., Fischer, J., Wibaux, M., 2004. Circulation and deep water export at the western exit of the subpolar North Atlantic. Journal of Physical Oceanography 34, 817–843.

Schott F.A., Fischer, J., Dengler, M., Zantopp, R., 2006. Variability of the Deep Western Boundary Current east of the Grand Banks. Geophysical Research Letters 33 [doi:10.1029/2006GL026563].

Smethie, W.M., Fine, R.A., 2001. Rates of North Atlantic Deep Water formation calculated from chlorofluorocarbon inventories. Deep-Sea Research I 48, 189–215.

Spall, M.A., 2004. Boundary currents and water mass transformation in marginal seas. Journal of Physical Oceanography 34, 1197–1213.

Spall, M.A., Pickart, R.S., 2003. Wind driven recirculations and exchanges in the Labrador and Irminger seas. Journal of Physical Oceanography 33, 1829–1845.

Stouffer, R.J., Yin, J., Gregory, J.M., Dixon, K.W., Spelman, J.M., Hurlin, W., Weaver, A.J., Eby, M., Flato, G.M., Hasumi, H., Hu, A., Jungclaus, J.H., Kamenkovich, I.V., Levermann, A., Montoya, M., Murakami, S., Nawrath, S., Oka, A., Peltier, W.R., Robitaille, D.Y., Sokolov, A., Vettoretti, G., Weber, S.L., 2006. Investigating the causes of the response of the thermohaline circulation to past and future climate changes. Journal of Climate 19, 1365–1387.

Stramma, L., Kieke, D., Rhein, M., Schott, F., 2004. Deep water changes at the western boundary of the subpolar North Atlantic during 1996 to 2001. Deep-Sea Research I 51, 1033–1056.

Straneo, F., 2006. On the connection between dense water formation, overturning and poleward heat transport in a convective basin. Journal of Physical Oceanography 36, 1822–1840.

Straneo, F., Pickart, R.S., Lavender, K., 2003. Spreading of Labrador Sea Water: an advective–diffusive study based on Lagrangian data. Deep-Sea Research I 50, 701–719.

Talley, L.D., McCartney, M.S., 1982. Distribution and circulation of Labrador Sea Water. Journal of Physical Oceanography 12, 1189–1204.

Treguier, A.M., Theetten, S., Chassignet, E.P., Penduff, T., Smith, R., Talley, L., Beismann, J.O., Böning, C.W., 2005. The North Atlantic subpolar gyre in four high-resolution models. Journal of Physical Oceanography 35, 757–774.

Trenberth, K.E., Caron, J.M., 2001. Estimates of meridional atmosphere and ocean heat transports. Journal of Climate 14, 3433–3443.

Vellinga, M., Wood, R.A., 2002. Global climatic impacts of a collapse of the Atlantic thermohaline circulation. Climatic change 54, 251–267.

Willebrand, J., Barnier, B., Böning, C., Dieterich, C., Killworth, P.D., Provost, C.L., Jia, Y., Molines, J., New, A.L., 2001. Circulation characteristics in three eddy-permitting models of the North Atlantic. Progress in Oceanography 48, 123–161.